Progress In Electromagnetics Research M, Vol. 112, 217–230, 2022

Demonstration and Performance Appraisal of Calibration Network for Multi-Element Calibration in Active Phased Array

Virendra Kumar[1, 2, *], Chakkandan A. Sreejith[1], Shreeshail[1], Upendra S. Pandey[1], Karukunnel S. Beenamole[1], and Ravi K. Gangwar[2]

Abstract—In active phased arrays, T/R module performance drifts due to active components' aging and thermal effect. Hence periodic online field calibration is required during the deployment of a radar system. This paper presents an innovative design of a precise and consistent calibration network consisting of a buried leaky coaxial cable (LCX) and a calibration switch network (CSN) for fast periodic field calibration of an active phased array. In the antenna plate, the leaky coaxial cables are buried within the wall of the cavity-backed antenna to realize calibration lines. A calibration switching network is realized using a $1:30$ way Wilkinson power divider/combiner for simultaneous excitation of multiple calibration lines to characterize multiple radiating elements in the active array. An S-band ($3.3\,\text{GHz} \pm 200\,\text{MHz}$) experimental active array with 64 T/R modules is configured and tested in the near-field test range (NFTR) to demonstrate the performance of the proposed calibration network. The presented scheme of simultaneous calibration of multiple radiating elements significantly reduces array calibration time and provides more flexibility to other multifunction radar functions. The availability of multiple receivers and non-overlapping RF beam forming networks in the radar system limits the improvement factor in array calibration time mentioned in this paper.

1. INTRODUCTION

Active phased array antenna consists of radiating elements, T/R modules, and beamforming network. The insertion phase misalignment in the excitation of radiating elements due to the active/passive components of the active phased array degrades array directivity, fills the sidelobe nulls, and severely affects the average sidelobe level (SLL). The symmetrical design of the beamforming network to match the electrical line lengths of each radiating element and the production of insertion matched T/R modules for an active array is a costly and tedious process. The imperfection in the active array element excitation can be eliminated by adjusting the electrical length of the radiating elements. Therefore, the calibration network becomes a viable solution for active phased array radars and phased array communication systems.

Seker [1] describes the most common phased array calibration methods, i.e., near-field scanning probe, peripheral fixed probes, calibration lines, and mutual coupling, along with their advantages and disadvantages. These calibration methods are time-consuming due to the sequential measurement of the active array's insertion characteristics of radiating elements. A transmission line based built-in performance-monitoring/fault isolation and correction (PM/FIC) as a calibration network for active phased array calibration has large coupling variation [2, 3]. The phased array calibration techniques without a calibration network are also explained [4–8], in combination with signal processing techniques

Received 16 March 2022, Accepted 28 July 2022, Scheduled 17 August 2022

* Corresponding author: Virendra Kumar (virendra.kumar@lrde.drdo.com).

[1] Electronics and Radar Development Establishment (DRDO), Bangalore-560093, India. [2] Department of Electronics Engineering Indian Institute of Technology (Indian School of Mines), Dhanbad-826004, India.

by using the element excitation method (EEM), phase-match method (PMM), and multi-element phase-toggle (MEP) method. These signal processing techniques are either time-consuming or computationally extensive and unsuitable for large antenna arrays. Multi-element phased array calibration method by solving linear equations [9, 10] is very complicated and simultaneously calibrates a maximum of eight elements; another computational extensive synthetic array calibration (SAC) scheme [11] offers only 1.7 times reduction in the calibration time compared to single element calibration methods [1]. The fast measurement technique for multi-element phased array calibration is presented in [12–14], which suffers from large measurement error and calibration accuracy. To achieve low root-mean-square error (RMSE) in multi-element calibration, these methods require multiple measurements and computationally extensive algorithms, thereby a significant increase in calibration time. Therefore, the limitations of the reported phased array calibration network and calibration procedures are not suitable for calibrating large antenna arrays of long-range search and tracking radars.

Theoretical analysis and radiation characteristics of the leaky coaxial cables with periodic slots are well established and presented [16]. In [17], a leaky coaxial cable (LCX) as a buried calibration line is presented as a coupler for active phased array calibration. This paper is an extension of [17] and presents an innovative design of a calibration network as a built-in mechanism for the simultaneous calibration of multiple radiating elements. In this proposed design, leaky coaxial cables (LCXs) are buried as calibration lines within the cavity-backed antenna element wall and act as a coupler for active phased array calibration [17]. In contrast, the calibration switch network (CSN) has a mechanism for the simultaneous excitation of calibration lines for multi-element calibration. The proposed calibration network is realized and evaluated in the near-field test range (NFTR) to determine the calibration coefficient for the successful calibration of a 64-element experimental array. This paper presents an analytical framework for calibrating a large active phased array with the proposed calibration network, significantly reducing active array online/off-line calibration time and improving radar system performance.

2. ACTIVE PHASED ARRAY CALIBRATION NETWORK

A typical active phased array configuration shown in Fig. 1 consists of a calibration network, T/R modules, RF manifold, exciter, and multichannel receiver (EMCR). The proposed calibration network is entirely passive and consists of an RF feed network, a 1 : 2 way power divider, a CSN, and buried LCXs as calibration lines. In this present antenna configuration, the active array has 14 independent receive channels in the EMCR; hence, a multistage RF manifold (an analog beamforming network) is designed considering the limitation of available independent receive channels in the EMCR. The EMCR also generates a CAL signal at the intended frequency and feeds it to the calibration network in the receive calibration. In the forward path (receive calibration), CSN distributes the CAL signal as per the selective excitation of a group of LCXs and exhibits minimum insertion. In the reverse direction, the T/R module's transmitting signal is coupled by LCXs, and the CSN circulator routes the coupled signal to the high-power attenuator path. The high power attenuator in the CSN prevents the EMCR receiving channel from saturation/damage during transmit calibration.

2.1. Initial Transfer Function (ITF) of Calibration Network

The ITF is measured in the NFTR as S-parameters of an active array by injecting an RF signal in the calibration network, i.e., coupling between the radiating elements and LCXs, insertion characteristics of CSN, and its RF feed network. The proposed calibration network is entirely passive and consists of an RF feed network, a 1:2 way power divider, CSN, and buried LCX are as calibration lines. Hence it is presumed that insertion characteristics of the calibration network are relatively constant for the intended lifespan of the active array antenna; thus, the radar system stores it as a reference for periodic online field calibration of an active phased array [2, 8]. The active array has $m \times n$ active elements as shown in the active phased array architecture block diagram with M buried calibration lines, where $M = 1 \ldots 60$, $m = 1 \ldots 120$ (columns in the antenna array), and $n = 1 \ldots 96$ (rows in the antenna array). While the S-parameter of an $(m \times n)$th active element are measured, all the remaining ports in the active array must be terminated by a matched load (i.e., $50\,\Omega$ loads or T/R modules). In the

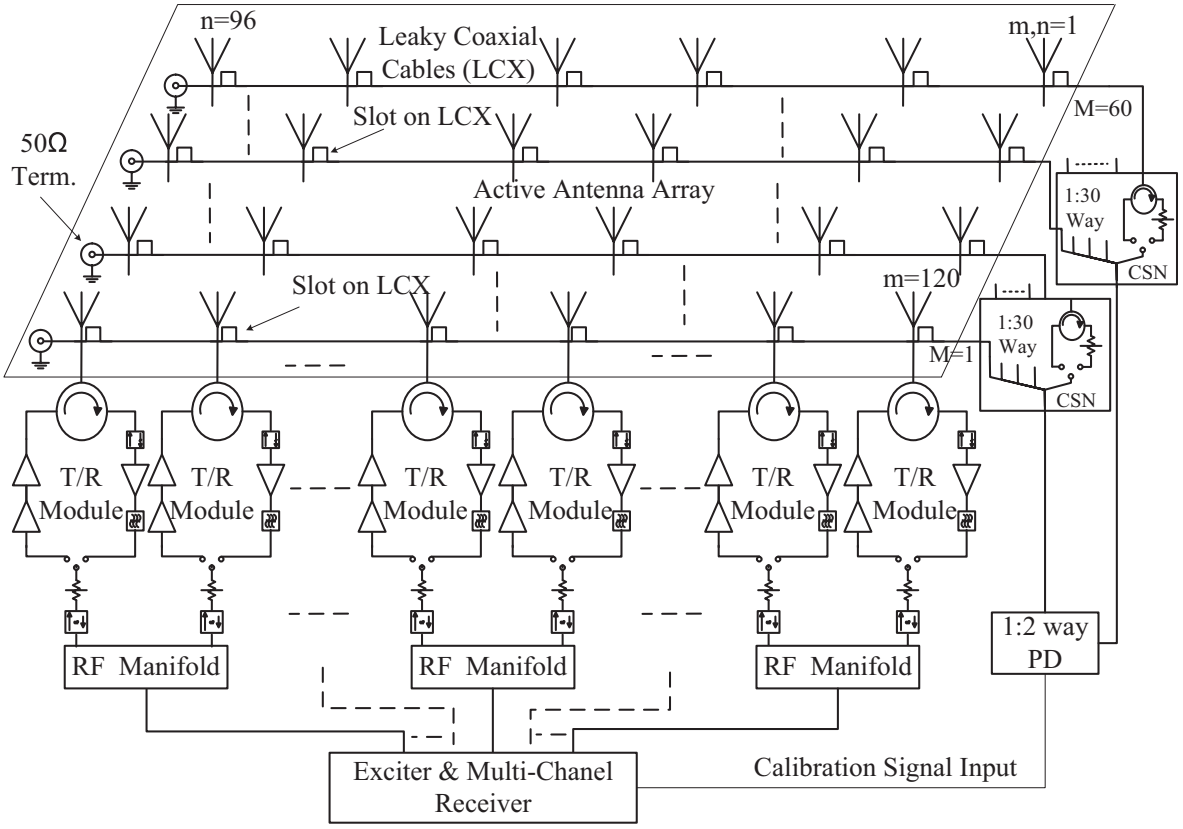

Figure 1. The block diagram of an active phased array architecture with the proposed calibration network (CSN and embedded LCXs).

active array, calibration line ports and radiating elements can be represented using the general form of the scattering matrix as follows:

$$|b| = |S||a| \tag{1}$$

where $a = (a_1, a_2, \ldots, a_N)$ and $b = (b_1, b_2, \ldots, b_N)$ are the generalised incident and reflected wave in an N-port network, where N is the total number of ports in the active phased array antenna.

$$\begin{bmatrix} b_1 \\ b_2 \\ \vdots \\ b_N \end{bmatrix} = \begin{bmatrix} S_{11} & S_{12} & \ldots & S_{1N} \\ S_{21} & S_{22} & \ldots & S_{2N} \\ \vdots & \vdots & \ldots & \vdots \\ S_{N1} & S_{n2} & \ldots & S_{NN} \end{bmatrix} \begin{bmatrix} a_1 \\ 2 \\ \vdots \\ a_N \end{bmatrix} \tag{2}$$

Therefore,

$$S_{ij} = \left.\frac{b_i}{a_j}\right|_{a_k=0 \; for \; k \neq j} \tag{3}$$

where S_{ij} is defined as the ratio of the reflected wave at port i to the incident wave at port j.

Figure 2 explains the calibration network's ITF measurement setup in NFTR. As shown in Fig. 2, the calibration network consists of interconnect RF cables, power dividers, CSN, and the coupling from LCX to the radiating element. The entire calibration network is measured and characterized in terms of calibration coefficient using the factory's NFTR [4, 6, 20].

Due to the separation of scanner probe to radiating element, signal path loss and phase delay for the distant d are represented as free space path loss and phase delay;

$$Path\,loss: \; L_d = \left[\frac{4\pi d}{\lambda}\right]^2 \qquad Phase\,delay: \angle L_d = \phi_{L_d} = 2\pi d/\lambda \tag{4}$$

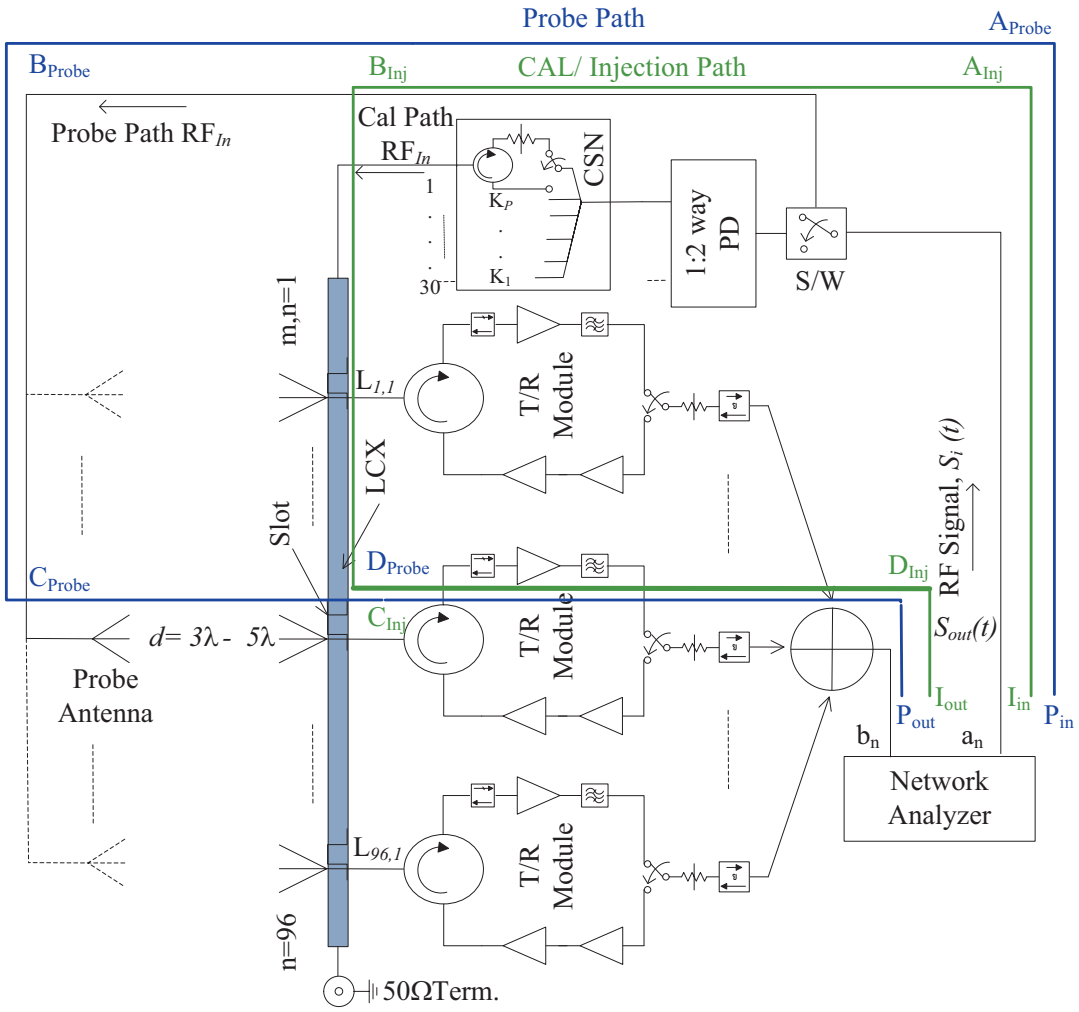

Figure 2. Calibration network's ITF measurement setup in NFTR.

Insertion loss and phase delay in the RF manifold network are considered as transmission loss and transmission delay, which is a reciprocal S-matrix;

$$L_t = \begin{bmatrix} 0 & e^{-\gamma l} \\ e^{-\gamma l} & 0 \end{bmatrix} \tag{5}$$

where $\gamma = \alpha + j\beta$ is the complex propagation constant, α the line attenuation in [neper/m], and $\beta = 2\pi/\lambda$ with the operating wavelength λ.

As shown in Fig. 2, the NFTR scanner moves sequentially to the coordinates of the element under test (EUT) in the array grid and measures the transmission coefficient of each element by exciting the probe path ($P_{in} \rightarrow A_{Probe} \rightarrow B_{Probe} \rightarrow C_{Probe} \rightarrow D_{Probe} \rightarrow P_{out}$). The probe antenna transmits a single-tone RF sinusoidal signal which is received by the element under test. The received signal is amplified and combined through the beamforming network. Similarly, to measure the transmission coefficient of the antenna through the CAL/Injection path ($I_{in} \rightarrow A_{Inj} \rightarrow B_{Inj} \rightarrow C_{Inj} \rightarrow D_{Inj} \rightarrow I_{out}$), a single-tone RF sinusoidal signal is injected at the calibration port of the calibration network [6, 10]. The measurement of the transmission coefficient of each element is performed in the receiving mode of the antenna by sequentially switching 'on' one T/R module at a time, whereas the remaining T/R modules shall be in the high isolation stage in the array. The measured signal from the probe and calibration path is represented as follows;

$$\text{Probe path signal}: \quad P_{m,n}(t) = L_d L_{l_p} G_{T_{m,n}} \exp\{-j(\phi_{L_d} + \phi_{L_{l_p}} + \phi_{T_{m,n}})\} S_i(t) \tag{6a}$$

$$\text{CAL path signal}: \quad I_{cal_{m,n}}(t) = K_p L_{m,n} L_{l_c} G_{T_{m,n}} \exp\{-j(\phi_{K_p} + \phi_{L_{m,n}} + \phi_{L_{l_c}} + \phi_{T_{m,n}})\} S_i(t) \tag{6b}$$

where $P_{m,n}(t)$ and $I_{cal_{m,n}}(t)$ are signal received at sum port of array from the probe path and calibration network path, respectively. L_{l_p} and L_{l_c} are RF manifold losses in probe and calibration network path. K_p, $L_{m,n}$, and $G_{T_{m,n}}$ are insertion loss of CSN for the pth path, LCX to radiating element coupling for (m,n)th element, and gain for (m,n)th T/R module, respectively. Similarly, $\phi_{L_{l_p}}$ and $\phi_{L_{l_c}}$ are RF manifold insertion phase in probe and calibration network path. ϕ_{K_p}, $\phi_{L_{m,n}}$, and $\phi_{T_{m,n}}$ are insertion phase of CSN for the pth path, LCX to radiating element coupled insertion phase for (m,n)th element, and insertion phase for (m,n)th T/R module, respectively.

The calibration network's ITF is obtained for each radiating element as the ratio of probe path to injection path transmission coefficients. The calibration network's ITF $C_{m\cdot n}$ for all the radiating elements can be calculated by dividing Eq. 6(a) with Eq. 6(b) and can be written as follows

$$C_{m,n} = \frac{P_{m,n}(t)}{I_{cal_{m,n}}(t)} = \frac{L_d L_{l_p} \exp\{-j(\phi_{L_d} + \phi_{L_{l_p}})\}}{K_p L_{m,n} L_{l_c} \exp\{-j(\phi_{K_p} + \phi_{L_{m,n}} + \phi_{L_{l_c}})\}} \tag{7}$$

$C_{m\cdot n}$ is the calibration reference data for periodic online field calibration of the active phased array. A single-tone RF sinusoidal signal is injected at the calibration port while field calibration is performed. To calculate the amplitude and phase error in the active path of (m,n)th element, $C_{m\cdot n}$ is multiplied with the beamforming network's sum port signal [3].

$$I'_{cal_{m,n}}(t) = \delta G_{m,n} \exp\{-j(\delta\phi_{G_{m,n}})\} I_{cal_{m,n}}(t) \tag{8a}$$

$$P'_{m,n}(t) = C_{m,n} \times I'_{cal_{m,n}}(t) \tag{8b}$$

$$P'_{m,n}(t) = G_k \delta G_{T_{m,n}} \exp\{-j(\phi_k + \delta\phi_{T_{m,n}})\} \tag{8c}$$

where $\delta G_{m,n}$ and $\delta\phi_{G_{m,n}}$ are the relative change in the injection path amplitude and phase corresponding to the (m,n)th element attributed to the repair or replacement of T/R modules in the active array. The active array is under calibration at time instant t, and $\delta G_{T_{m,n}}$ and $\delta\phi_{T_{m,n}}$ are the relative change/deviation in amplitude and phase corresponding to the (m,n)th T/R modules in the active array. The amplitude change/deviation are adjusted to the mean value using a digital attenuator across the elements, whereas phase change/deviation are brought to zero by setting phase shifters limited to their quantization errors [2, 7, 8]. G_k and ϕ_k are the constant gain and phase factor common for all elements, normalized during the calibration process.

Since all the LCXs are subjected to a uniform environment and age equally in the radar system, the change in the electrical properties of all the LCXs is proportional to their initial electrical values, i.e., tracking of cable loss and insertion phase. The relative change in the electrical properties of all the LCXs is treated as a constant variation and does not alter the relative coupling between the LCX and radiating element in the active array. Therefore, ITF remains valid for online/off-line field calibration of an active phased array for an intended lifespan of the active phased array. Hence, the radar system stores it as a reference for periodic online field calibration of an active phased array [2, 8].

3. DESIGN OF EMBEDDED CALIBRATION NETWORK

A precise and stable, embedded calibration network is realized with minimal modification in the radiating elements without degrading the radiation performance. The proposed calibration network works as a built-in closed-loop circuit for T/R module failure identification and field calibration of an active phased array without returning to NFTR or bringing expensive far-field test equipment to recalibrate the active array [3, 4].

3.1. Leaky Coaxial Cable (LCX)

In this proposed design of LCX as the calibration line, a small amount of RF signal leaks and couples to the radiating element. The design requires two slots to meet the design goal of $-50\,\text{dB} \pm 10\,\text{dB}$ to

coupling/leak RF signal to each radiating element. Since the leaky coaxial cable couples a very weak RF signal at the site of each radiating element, it does not affect the radiation performance of the antenna array. Here, a standard hand-formable coaxial cable is used to realize leaky coaxial cable by removing the outer shield/conductor to probe/feed RF signal to/from the radiating element.

As shown in Fig. 3, one calibration line is common for the two columns of radiating elements. These coaxial cables are buried within the wall of the cavity-backed antenna element to form a calibration line [17]. The buried cables are machined at two locations with the dimension of 4×1.2 mm to remove the outer conducting shield corresponding to each radiating element. Due to slot discontinuity in coaxial cables, a portion of the energy is reflected, resulting in a slight degradation in the return loss [15–17].

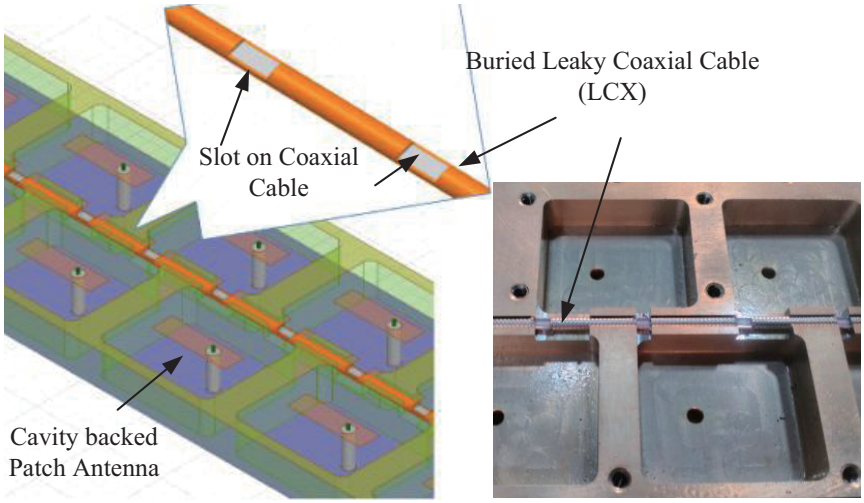

Figure 3. Design and realization of buried LCX as embedded calibration lines in the cavity-backed patch antenna.

An experimental antenna array with four 6 m long vertical LCXs is realized for an antenna array having ninety-six rows and eight columns. The realized calibration lines are measured from 3.1 GHz to 3.5 GHz at five spot frequencies in the lab with an Agilent N5241A network analyzer. The calibration line's input-output port return loss is better than 10 dB, as shown in Figs. 4(a) and (b) having 192 slots. The LCX exhibits a maximum insertion loss of 6.02 dB at 3.5 GHz presented in Fig. 4(c) for 6 m long LCX. The LCX to radiating element coupling is achieved from −48 dB to −58 dB within 10 dB variation as shown in Fig. 4(d) to reduce dynamic range requirement during online/off-line phased array calibration of the active antenna [12].

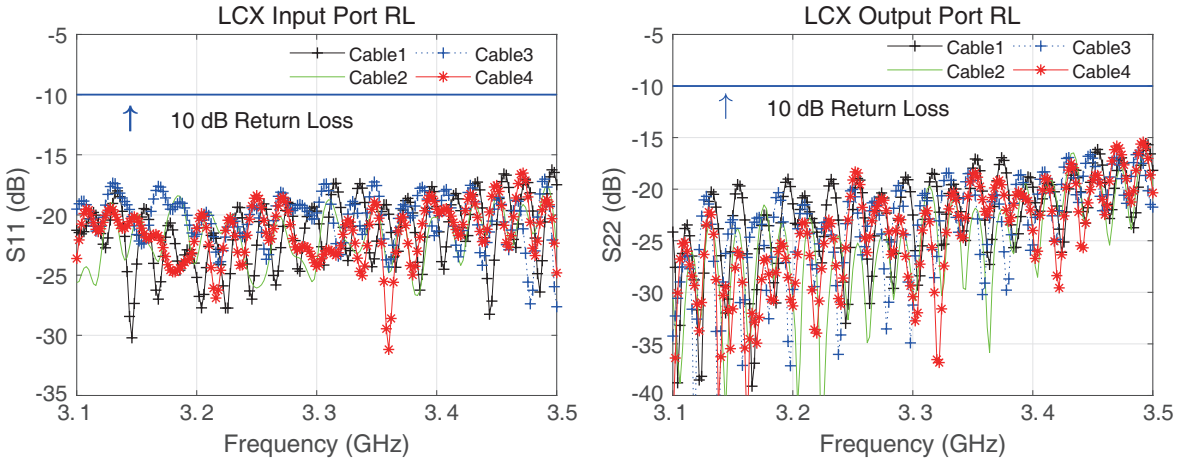

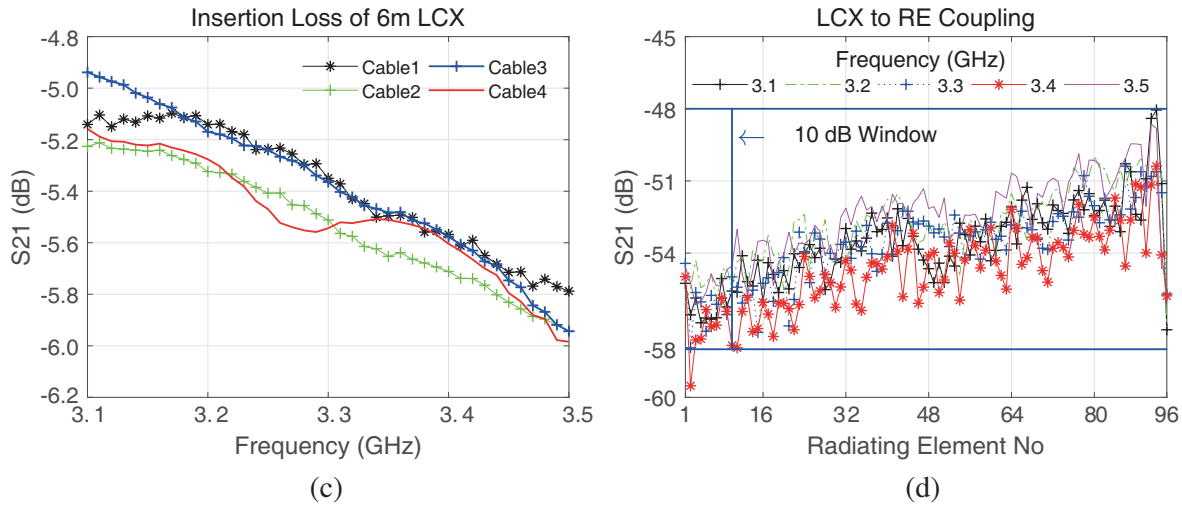

Figure 4. (a) LCX input port-1, S_{11}, (b) LCX output port-2, S_{22}, (c) insertion loss S_{21} of 6 m long LCX, and (d) LCX to radiating element CAL coupling S_{21}.

3.2. Calibration Switch Network (CSN)

A CSN is designed for simultaneous excitation of multiple calibration lines to enable multi-element calibration to significantly reduce active array calibration time [13, 14]. A general block diagram of the proposed design of CSN is shown in Fig. 5. In this unique design of 1 : 30 port, Wilkinson power divider/combiner [18], every port has high power low loss reflective switches (SPDT) [19] for selective excitation of an individual or a group of calibration lines. A high-power surface mount attenuator [20] is placed in the reverse path to protect EMCR during transmit calibration. The circulator at every output port makes it a bidirectional design for receiving and transmitting calibration [21]. An FPGA-based

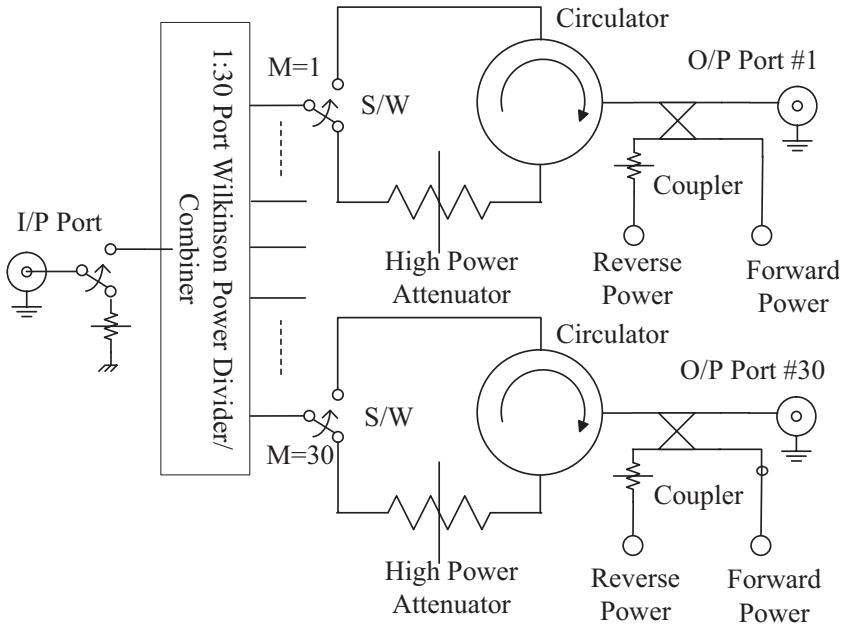

Figure 5. Block diagram of 1 : 30 way bidirectional CSN with inbuilt fault monitoring and identification functionality.

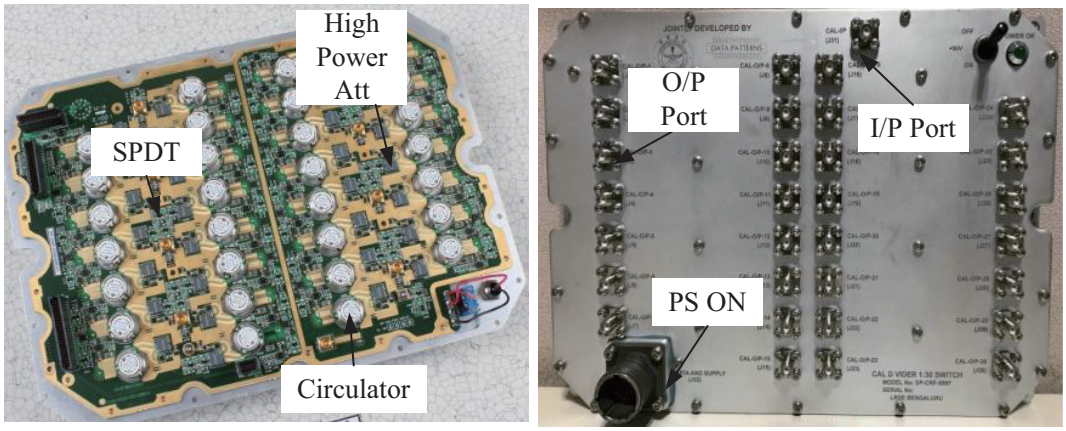

Figure 6. CSN realization on multilayer RT@duroid and FR4 laminate.

controller sets the CSN switches either in the conduction path or in an isolation path within 0.5 µs and reports their status during the array calibration. Fig. 6 shows the realized CSN hardware on multilayer laminate (RT@duroid and FR4) to route RF and digital controls signals.

The performance of CSN is measured in the lab using an N5241A network analyzer. As shown in Fig. 7(a) and Fig. 7(b), CSN exhibits a maximum 20.5 dB to 22.2 dB insertion loss in the forward path and a minimum 36.0 dB port to port isolation from 3.1 GHz to 3.5 GHz frequency. Amplitude and phase balance (power and phase difference between the two output ports) among all the 30 ports is within ±1.0 dB and ±5.0 deg shown in Figs. 7(c) and (d) respectively for the entire 400 MHz bandwidth.

4. ACTIVE PHASED ARRAY CALIBRATION

Phased array calibration matches the insertion characteristics of each radiating element by adjusting the electrical length of all radiating elements via digital phase shifters and attenuators and eliminates imperfection in active antenna excitation [4–8].

4.1. Proposed Calibration Network & Measured Results

The ITF of the calibration network is measured in the near-field test facility as per the process described in Section 2.1 to calibrate a 64-element experimental array. The ITF of the experimental antenna is presented in Figs. 8(a) and (b), and the insertion amplitude and phase vary from −38 dB to −48 dB

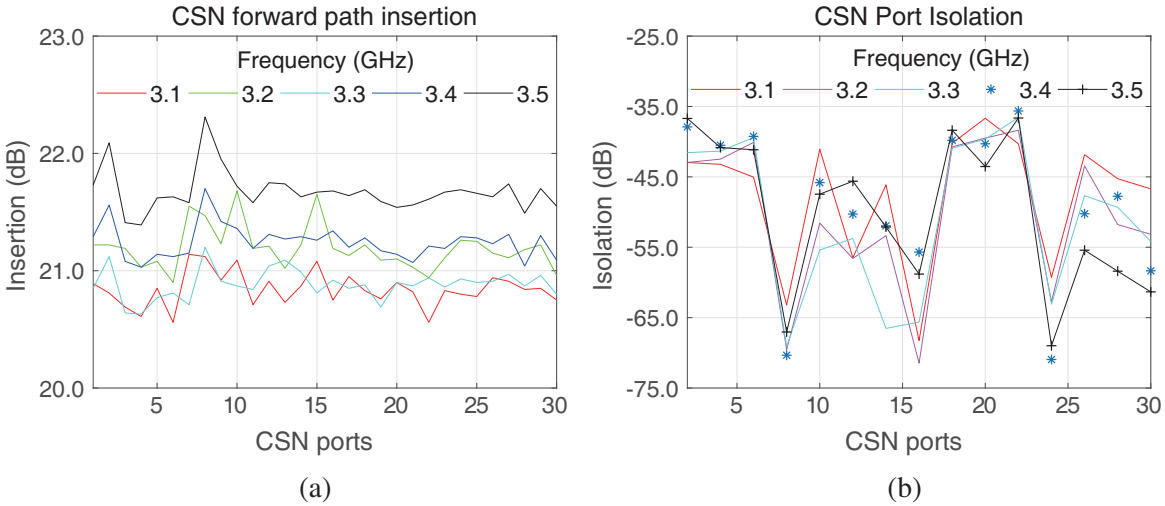

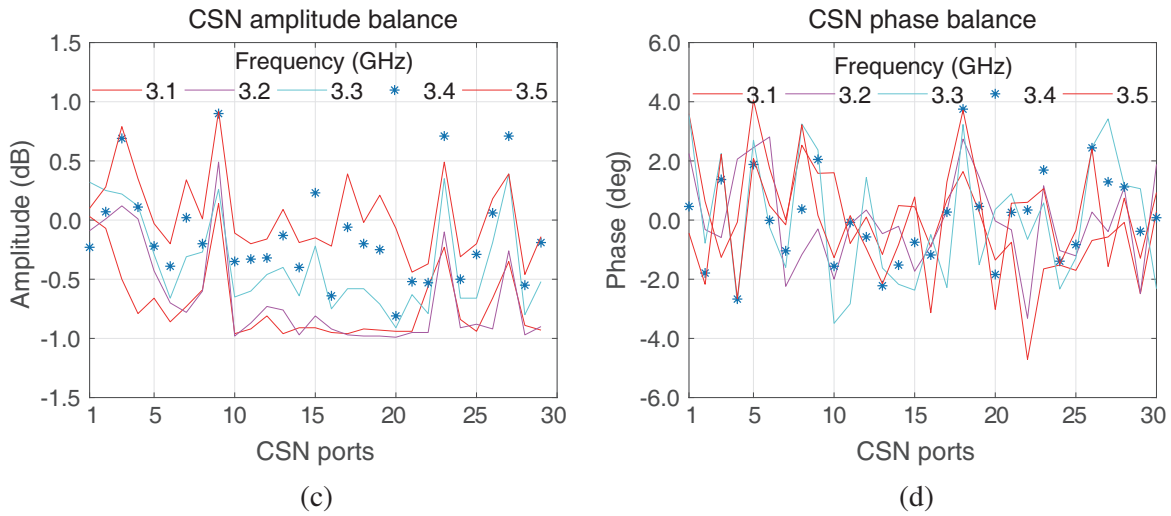

Figure 7. Measured performance of CSN (a) forward insertion loss, (b) port to port isolation, (c) amplitude, and (d) phase balance over 400 MHz bandwidth.

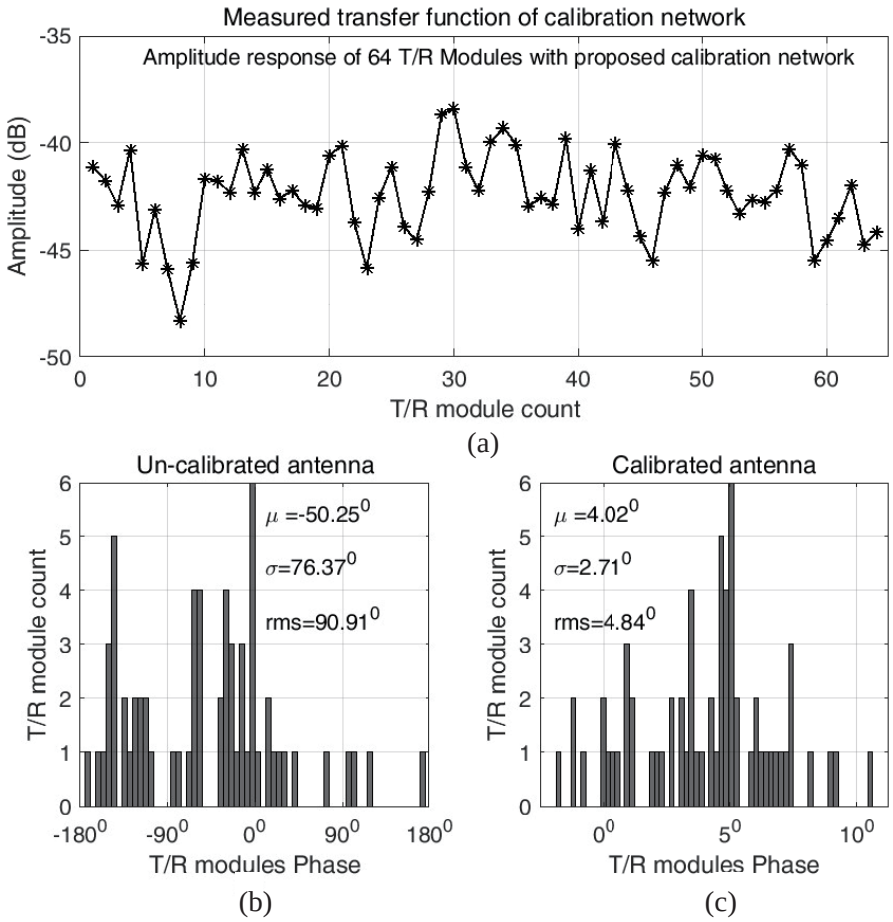

Figure 8. (a) Measured ITF of proposed calibration network for 64 elements active array, (b) uncalibrated array phase errors, (c) calibrated array phase error.

and −180 deg to +180 deg, respectively, corresponding to 64 active elements. Phase-only calibration of the experimental array was carried out by using the proposed calibration network. In Figs. 8(b) and (c), measured results are presented for the calibrated and un-calibrated experimental arrays. Measured results show that an un-calibrated active phased array has 90 deg, RMS phase error with an std of 76.37 deg and 50.25 deg mean on antenna aperture. On the other hand, the calibrated active array has 4.84 deg, RMS phase error with an std of 2.71 deg and 4.02 deg mean on the antenna aperture.

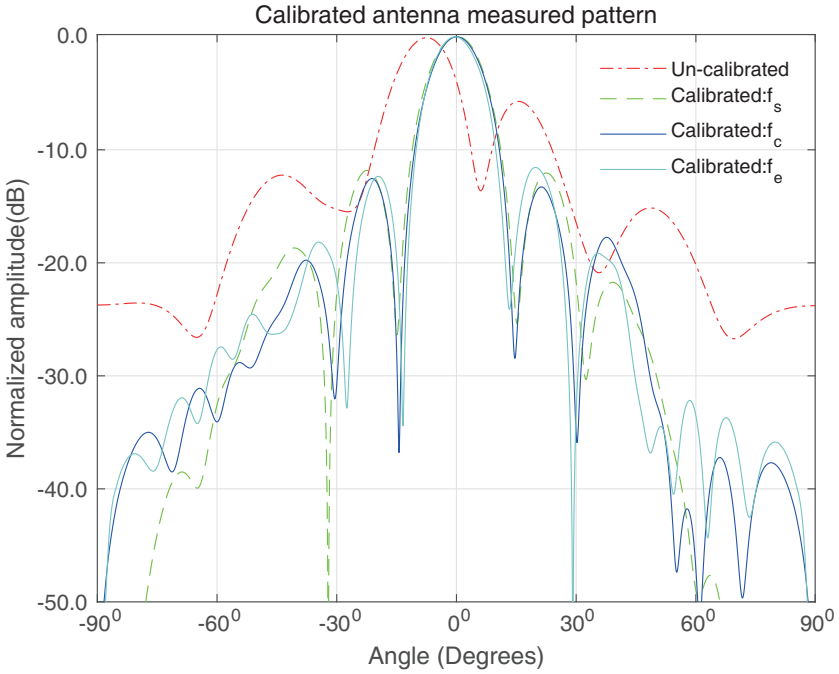

Figure 9. Measured pattern of un-calibrated and phase only calibrated active phased array.

The radiation performance of the un-calibrated and calibrated experimental antenna arrays is measured in NFTR and presented in Fig. 9. The measured results infer that the un-calibrated antenna array has an undefined beam pattern with a lower antenna array gain. The radiation pattern shows that antenna array nulls are filled and have very poor sidelobes performance. On the other hand, the calibrated antenna array has a narrow antenna beam with high gain, proper null definition, and better sidelobes. The measured results are presented in Table 1 which successfully demonstrate and validate the proposed calibration network for an active phased array [3].

Table 1. Radiation parameters of un-calibrated and calibrated experimental array.

Measured Parameters	[a]BPE (degrees)	Beam Width (degrees)	Peak SLL (dB)	Directivity (dB)
Un-Collimated	$-7.4/-0.65$	13.79/9.92	$-5.64/-8.89$	16.92
f_s: Collimated	$-0.19/-0.46$	13.33/11.79	$-11.68/-13.85$	23.43
f_c: Collimated	$-0.08/+0.12$	12.34/10.91	$-13.99/-14.82$	24.11
f_e: Collimated	$+0.33/+0.19$	12.15/10.19	$-11.49/-13.43$	24.23

[a] beam pointing error (BPE)

5. MULTI-ELEMENT CALIBRATION SCHEME

Generally, in an active array, the transmission coefficient of each radiating element is measured sequentially by switching 'on' one T/R module at a time, whereas the remaining T/R modules shall be in the high isolation stage. The presented antenna array, as shown in Fig. 10, is configured with 96 rows and 112 columns as active elements. It is evident from the array configuration presented in Section 2 that in each non-overlapped RF manifold channel, one LCX can be excited, and only one T/R module can be switched 'on' for array calibration. Therefore, the transmission coefficient of 14 radiating elements is measured simultaneously to minimize active array online/off-line calibration time. The calibration process requires the transmission coefficient of all the elements in the antenna array; hence the process is repeated for the remaining elements.

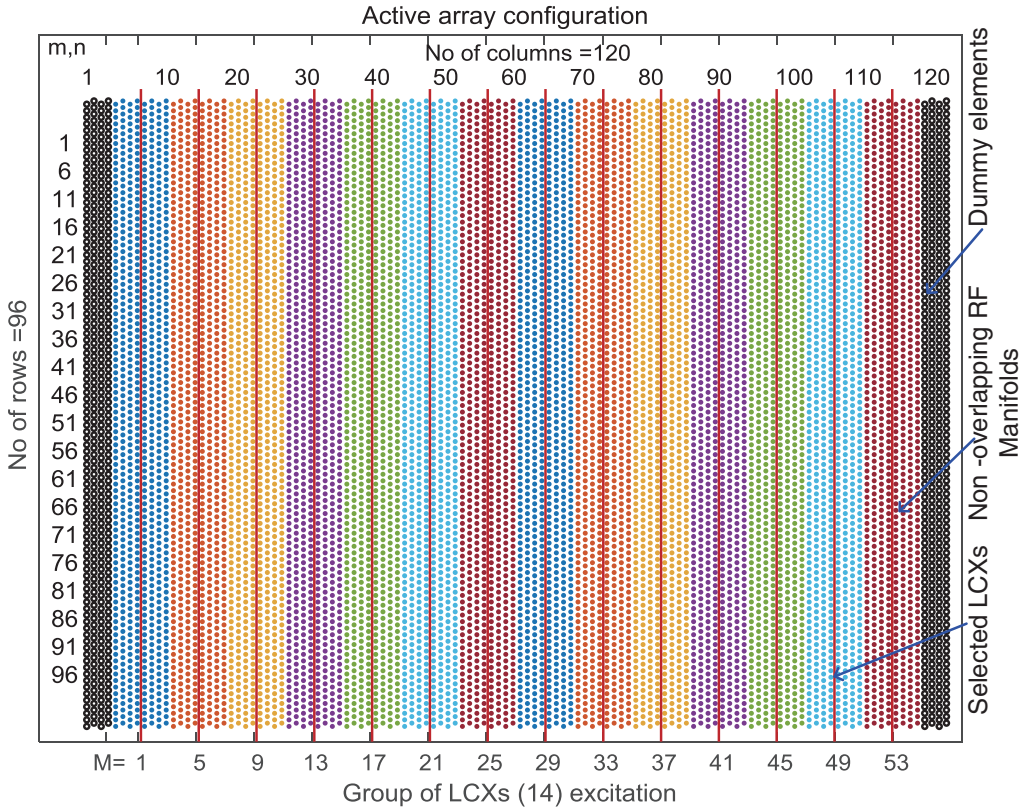

Figure 10. Simultaneous excitation of multiple calibration lines to calibrate multiple T/R modules in the presented array configuration.

5.1. Performance Improvement in Array Calibration

The proposed calibration network presented in this paper enables multi-element calibration in an active array. The required calibration time for the sequential calibration of one-by-one radiating element vs. simultaneous excitation of multiple radiating elements is computed and presented for 10000 elements, active array in Table 2. The computational results demonstrate that the calibration of one-by-one radiating elements requires 128.96 minutes, whereas simultaneous calibration of 14 radiating elements requires 11.69 minutes for an identical set of frequencies, beam types, and number of iterations. Hence, the proposed calibration scheme demonstrates an 11-fold improvement in array calibration time.

In this active array architecture, the T/R modules receive control commands over 10 Mbps universal asynchronous receiving/transmitting (UART) interface. A selected group of T/R modules is set in the calibration mode for simultaneous calibration through the UART interface. Therefore, the

Table 2. Active array calibration time computation.

On-line Calibration Parameters	Single Element	Multiple Element	Units /No.
No. of antenna elements	10000	10000	*no.*
No of array control modules	296	296	*no.*
Single burst duration	1.6	1.6	*milli* sec
No of T/R module under calibration	1	14	*no.*
Calibration computation time	10	10	*milli* sec
Total time per iteration	483.6	43.83	*milli* sec
No of iterations/ beam type	5	5	*no.*
Calibration time per beam type	2418	219.14	*milli* sec
No of antenna beam types	4	4	*no.*
Total time per spot frequency	9.67	0.88	sec
No of frequencies	32	32	*no.*
Total calibration time	5.16	0.47	*minutes*
On-line calibration time budget	2	2	%
Search frame time	4	4	sec
Available time for calibration	0.08	0.08	sec
Time required for calibration	483.6	43.83	sec
No of operational frequencies	16	16	*no.*
Total On-line calibration time	128.96	11.69	*minutes*

communication overheads to control multiple T/R modules limit improvement factor (14 no of T/R modules simultaneously switched 'on'). Hence, the improvement factor by 14 is not achievable due to the communication overheads in controlling the T/R modules. This work is compared with the previous work in Table 3, which shows significant improvement in system performance.

Table 3. Comparison with previous work.

	This work	[22]	[14]	[23]	[24]	[25]	[4]
Num. of elements	14	256	20	16	256	8	8
Meas. per elemenet	1	1	11.2	1.9	5.9	64	1
RMS Error (deg)	4.8	9.5	16.1	11	–	3	3
Orthogonal codes	No	Yes	No	No	Yes	Yes	Yes
Syncronization	Yes	No	No[a]	Yes	No	No[a]	Yes

[a] Although VNA is used, synchronization is not necessary in principle.

6. CONCLUSION

The realized calibration network disclosed in this paper enables the calibration of a deployed active phased array without returning to NFTR or bringing expensive far-field test equipment to recalibrate the active array. It exhibits excellent repeatability and facilitates a built-in closed-loop passive circuit to identify failures in active antennas. The proposed calibration network demonstrates simultaneous calibration of multiple radiating elements and achieves an 11-fold improvement in the active array calibration time allocated out of the radars search and track time budget. This improvement factor is not the limitation of the calibration network but a constraint of the availability of multiple receivers in the active array.

ACKNOWLEDGMENT

The authors acknowledge their gratitude towards the Director LRDE for support during the work.

REFERENCES

1. Seker, I., "Calibration methods for phased array radars," *Proc. of SPIE, Radar Sensor Technology XVII*, Vol. 8714, 87140W, May 31, 2013.
2. Lee, K.-M., R.-S. Chu, and S.-C. Liu, "A built-in Performance-Monitoring/Fault Isolation and Correction (PM/FIC) system for active phased-array antennas," *IEEE Transactions on Antennas and Propagation*, Vol. 41, No. 11, 1530–1540, Nov. 1993.
3. Chae, S. C., H. W. Jo, J. I. Oh, G. Kim, and J. W. Yu, "Coupler integrated microstrip patch linear phased array for self-calibration," *IEEE Antennas and Wireless Propagation Letters*, Vol. 19, No. 9, 1615–1619, Sept. 2020.
4. Salas-Natera, M. A., R. M. Rodriguez-Osorio, and L. de Haro, "Procedure for measurement, characterization, and calibration of active antenna arrays," *IEEE Trans. Instrum. Meas.*, Vol. 62, No. 2, 377–391, Feb. 2013.
5. Hampson, G. A. and A. B. Smolders, "A fast and accurate scheme for calibration of active phased-array antennas," *IEEE Antennas and Propagation Society International Symposium, 1999 Digest, Held in conjunction with: USNC/URSI National Radio Science Meeting (Cat. No. 99CH37010)*, Vol. 2, 1040–1043, Orlando, FL, 1999.
6. Hu, C., "A novel method for calibrating deployed active antenna arrays," *IEEE Trans. Antennas Propag.*, Vol. 63, No. 4, 1650–1657, Apr. 2015.
7. Babur, G., G. O. Manokhin, E. A. Monastyrev, A. A. Geltser, and A. A. Shibelgut, "Simple calibration technique for phased array radar systems," *Progress In Electromagnetics Research M*, Vol. 55, 109–119, 2017.
8. Kim, K. S., E. Yang, and N. H. Myung, "Self-calibration of an active uniform linear array using phase gradient characteristics," *IEEE Antennas and Wireless Propagation Letters*, Vol. 18, No. 3, 497-501, Mar. 2019.
9. Fadamiro, A. O., A. A. Semomhe, O. J. Famoriji, and F. Lin, "A multiple element calibration algorithm for active phased array antenna," *IEEE Journal on Multiscale and Multiphysics Computational Techniques*, Vol. 4, 163–170, 2019.
10. Long, R., J. Ouyang, F. Yang, W. Han, and L. Zhou, "Multi-element phased array calibration method by solving linear equations," *IEEE Transactions on Antennas and Propagation*, Vol. 65, No. 6, 2931–2939, Jun. 2017.
11. Keizer, W. P. M. N., "Fast and accurate array calibration using a synthetic array approach," *IEEE Trans. Antennas Propag.*, Vol. 59, No. 11, 4115–4122, Nov. 2011.
12. Keizer, W. P. M. N., "Fast and accurate array calibration using a synthetic array approach," *IEEE Trans. Antennas Propag.*, Vol. 59, No. 11, 4115–4122, Nov. 2011.
13. Hou, Y., H. Shang, M. Yang, and C. Jin, "Method of multichannel calibration for unmanned aerial vehicle surveillance radar," *The Journal of Engineering*, Vol. 2019, No. 21, 7864–7867, 2019.
14. Takahashi, T., Y. Konishi, S. Makino, H. Ohmine, and H. Nakaguro, "Fast measurement technique for phased array calibration," *IEEE Trans. Antennas Propag.*, Vol. 56, No. 7, 1888–1899, Jul. 2008.
15. Radiall, "Hand formable cable.141," Radiall p/n: C291 864 065 datasheet, Apr. 2019.
16. Wang, J. H. and K. K. Mei, "Theory and analysis of leaky coaxial cables with periodic slots," *IEEE Transactions on Antennas and Propagation*, Vol. 49, No. 12, 1723–1732, Dec. 2001.
17. Kumar, V., C. A. Sreejith, U. S. Pandey, K. S. Beenamole, and R. K. Gangwar, "Design investigation of leaky coaxial cable as coupler for active phased array calibration," *2019 IEEE Indian Conference on Antennas and Propagation (InCAP)*, 1–5, 2019.
18. Mini-Circuits, "Ultra-small Ceramic power splitter/combiner," SCN-2-35+ datasheet, Rev. D Mar. 2006.

19. Analog Devices, "High power, 44 W Peak, Silicon SPDT Reflective Switch, 0.7 GHz to 3.5 GHz," ADRF5130 datasheet, Rev. A Feb. 2017.
20. JQL Electronics Inc., "SMT Circulator," JCM3050T3550PV5-AST datasheet, Rev. A May 2018.
21. Anaren, "Surface mount attenuator 150 Watts," Model D150NA30C4 datasheet, Rev. B Apr. 2019.
22. Aoki, Y., S.-G. Yang, Y. Hwang, S. Kim, and Y. K. Kim, "Asynchronous 256-element phased-array calibration for 5G base station," *IEEE Microwave and Wireless Components Letters*, Vol. 31, No. 6, 798–801, Jun. 2021.
23. Nafe, A., A. H. Aljuhani, K. Kibaroglu, M. Sayginer, and G. M. Rebeiz, "In-situ self-test and self-calibration of dual-polarized 5G TRX phased arrays leveraging orthogonal-polarization antenna couplings," *2020 IEEE/MTT-S International Microwave Symposium (IMS)*, 1081–1084, 2020.
24. Gal-Katziri, M., A. Fikes, F. Bohn, B. Abiri, M. R. Hashemi, and A. Hajimiri, "Scalable, deployable, flexible phased array sheets," *2020 IEEE/MTT-S International Microwave Symposium (IMS)*, 1085–1088, 2020.
25. Hong, Z., S. Schonherr, V. Chauhan, and B. Floyd, "Free-space phased-array characterization and calibration using code-modulated embedded test," *2019 IEEE MTT-S International Microwave Symposium (IMS)*, 1225–1228, 2019.